*Cerebral Cortex*, February 2019;29: 573–585

**doi: 10.1093/cercor/bhx340**
Advance Access Publication Date: 29 December 2017
Original Article

ORIGINAL ARTICLE

# Reduced Local and Increased Long-Range Functional Connectivity of the Thalamus in Autism Spectrum Disorder

Dardo Tomasi[1] and Nora D. Volkow[1,2]

[1]National Institute on Alcohol Abuse and Alcoholism, Bethesda, MD 20892, USA and [2]National Institute on Drug Abuse, Bethesda, MD 20892, USA

Address correspondence to Dardo Tomasi, Ph.D, 10 Center Dr, Rm B2L124, Bethesda, MD 20892-1013, USA. Email: dardo.tomasi@nih.gov

## Abstract

It is hypothesized that brain network abnormalities in autism spectrum disorder (ASD) reflect local overconnectivity and long-range underconnectivity. However, this is not a consistent finding in recent studies, which could reflect the developmental nature and the heterogeneity of ASD. Here, we tested 565 ASD and 602 neurotypical (NT) males, and 91 ASD and 233 NT females using local functional connectivity density (lFCD) mapping and seed–voxel correlation analyses to assess how local and long-range connectivities differ in ASD. Compared with NT males, ASD males had lower and weaker age-related increases in thalamic lFCD, which were associated with symptoms of autism. *Post-hoc* seed–voxel correlation analyses for the thalamus cluster revealed stronger connectivity with auditory, somatosensory, motoric, and interoceptive cortices for ASD than for NT, both in males and in females, which decreased with age in both ASD and NT. These results document the disruption of local thalamic connectivity and dysregulation of thalamo-cortical networks, which might contribute to perceptual, motoric, and interoceptive impairments, and are also consistent with a developmental delay in functional connectivity in ASD.

**Key words:** ASD, brain development, brain laterality, age, sex differences, intelligence, brain networks, FCDM, fMRI, ABIDE

## Introduction

Autism spectrum disorder (ASD) is believed to result from an interaction between genetic, developmental, and environmental factors and has a current global prevalence of 1.5% in developed countries (Baxter et al. 2015). In addition to deficits in social interactions and communication (Frith 1989) and the presence of restricted stereotypical behaviors, people with ASD also present deficits in emotional, sensorimotor, cognitive (Ozonoff et al. 1991), and complex information processing (Minshew et al. 1997; Müller 2007). An early influential fMRI study reported that ASD subjects ($N = 17$) had hyperactivation in Wernicke's area, hypoactivation in Broca's area, and lower synchrony in the language network during language comprehension compared with neurotypical (NT) subjects (Just et al. 2004). Such findings were interpreted to reflect "local" overconnectivity and "long-range" underconnectivity in ASD (Belmonte et al. 2004). Studies on emotion processing in ASD supported the long-range underconnectivity of the fusiform face area (FFA), but contrary to the local overconnectivity hypothesis, local underconnectivity was also found within the FFA in ASD (Khan et al. 2013). Whereas the early studies support the long-range underconnectivity hypothesis in ASD, results from a survey of 32 fMRI studies suggest that methodological choices may have impacted the long-range underconnectivity findings (Müller et al. 2011).

"Resting-state" fMRI connectivity (rfMRI) studies support long-range underconnectivity among language regions (Cherkassky et al. 2006; Assaf et al. 2010; Abrams et al. 2013) and also among other brain regions (Monk et al. 2009; Weng et al. 2010; Anderson et al. 2011; Alaerts et al. 2014; Lee et al. 2016; von dem Hagen

et al. 2013) in ASD. However, other rfMRI studies in ASD have demonstrated long-range overconnectivity between brain regions (Monk et al. 2009; Ebisch et al. 2011; Di Martino et al. 2011; Cerliani et al. 2015; Fishman et al. 2015) or no differences in long-range connectivity when compared with controls (Tyszka et al. 2014). This lack of agreement likely reflects the modest sample size of the studies, the heterogeneity of ASD, and the increased variability of the resting-state condition in the presence of temporal changes in the degree of vigilance, arousal, and attention (Mason et al. 2007; Doucet et al. 2012; Liu and Duyn 2013; Shirer et al. 2012).

There is less evidence for local overconnectivity in ASD, a hypothesis that has remained relatively understudied by rfMRI at the macroscopic level (i.e., among neighbor voxels) and unexplored at the microscopic level because human fMRI is not capable of measuring "local" connectivity at the cellular level – that of synapses, columns, and reentrant circuits therein. Postmortem brain studies are required to assess microconnectivity and few histological studies have been done in ASD, which reported disrupted cortical patterns that could contribute to impairments in cortical neurocircuitry (Ecker et al. 2017). Recent rfMRI studies based on the regional homogeneity (ReHo) of the MRI signal reported both local under- and overconnectivity in different brain regions in ASD (Maximo et al. 2013; Itahashi et al. 2015; Dajani and Uddin 2016; Nair et al. 2017). However, these studies were limited by small samples sizes (largest rfMRI study included 50 ASD participants). To overcome the limitations of small sample studies in ASD, the Autism Brain Imaging Data Exchange initiative (ABIDE I and II) aggregated rfMRI and structural brain imaging data from a total of 1026 ASD subjects and 1130 controls collected at different institutions around the world (Di Martino et al. 2014).

To tackle the overwhelming computational demands of large imaging datasets, we recently proposed local functional connectivity density (lFCD) mapping (Tomasi and Volkow 2010), an ultrafast graph theory method that is ideal for quantifying local connectivity in large samples (Tomasi and Volkow 2011b, c, 2012a, 2012b, 2012d). The lFCD metric reflects the local hubness and energy demand of the brain tissue (Tomasi et al. 2013). The lFCD has high gray matter (GM) sensitivity and specificity (Tomasi et al. 2016a) and is the most resilient of the functional connectivity (FC) metrics to temporal dynamics (Tomasi et al. 2016b). Different to the popular hypothesis-driven seed–voxel correlation approach, data-driven lFCD does not require regional hypotheses (i.e., seed locations) and is ideal for exploratory studies in large datasets such as the ABIDE sample.

The goal of the present study is to test the local overconnectivity hypothesis at the macroscopic level using the lFCD metric in ASD subjects for the first time, capitalizing on the large sample of ASD and NT subjects of the ABIDE consortium. Based on recent findings of aberrant thalamic connectivity in 60 ASD children (Nair et al. 2015), temporal and motor thalamo-cortical hyperconnectivity in 228 ASD subjects (Woodward et al. 2017), and of increased subcortical–cortical connectivity in 166 ASD/Asperger's subjects (Cerliani et al. 2015), we hypothesized local thalamic underconnectivity and disrupted long-range thalamic connectivity with cortical regions (overconnectivity with sensory regions and underconnectivity with multimodal association cortices) in ASD. Because ASD may reflect atypical developmental trajectories and lateralization of white matter (WM) tracts in the brain (Travers et al. 2012), we further hypothesized slower maturation and differential lateralization of the thalamic lFCD in ASD.

## Materials and Methods

### Subjects

No experimental activity with any involvement of human subjects took place at the author's institutions. Data were drawn from the ABIDE I and II, publicly available image repositories (http://fcon_1000.projects.nitrc.org/indi/abide/) of individuals with ASD and NT subjects contributed by 23 international sites. The participants provided written informed consent and were scanned according to procedures approved by the local Institutional Review Boards (IRB) at each institution. The data were shared with the approval of the local IRB at each institution. The Office of Human Subjects Research Protections at the National Institutes of Health (NIH) approved the study.

Whereas the full age range of subjects in the ABIDE samples is 7–70 years, we restricted the study to an age range of 7–40 years because some of the ABIDE sites include very few subjects in the upper age range (40–70 years), which may result in skewing of age and cognitive aging. The high prevalence of autism in men (6 times higher for men than women) and the skewed age distribution of the female sample could also prevent testing the slower maturation hypothesis in ASD. Thus, females and males were analyzed separately to assess potential group differences in developmental trajectories.

Only rfMRI datasets with full-brain coverage and without excessive head motion (mean framewise displacement, $\langle FD \rangle < 0.2$ mm)(Van Dijk et al. 2012) from 565 ASD (15.3 ± 6.8 years old) and 602 NT (15.5 ± 6.4 years old; Table 1) males were included in the main study. There were no differences in age between groups ($P = 0.63$; $t$-test). The standard full intelligence quotient (FIQ) was lower for ASD subjects (FIQ = 106 ± 16) than for NT subjects (FIQ = 113 ± 12; $P < 10^{-15}$; $t$-test). The female sample included 91 ASD (15.5 ± 9.1 years) and 233 NT (14.2 ± 7.5 years) women. Some of the ABIDE sites include the Autism Diagnostic Observation Schedule (ADOS) (Lord et al. 2000), a semi-structured assessment of communication, social interactions, and play, and the Autism Diagnostic Interview Revised (ADI-R) (Rutter et al. 2008), a structured interview conducted with the parents of ASD individuals. The ADOS total was the most consistently captured score across the ABIDE sites and was documented for 491 of the ASD individuals (440 men and 51 women; ADOS total = 11.3 ± 3.9; ADOS total scores did not differ significantly between men and women; $P = 0.86$). The social interaction score was the most consistently captured of the ADI-R scores across the ABIDE sites and was documented for 478 of the ASD individuals (416 men and 62 women; ADI-R social total = 19.5 ± 5.5; ADI-R social total scores did not differ significantly between men and women; $P = 0.90$).

Because different sites in the ABIDE consortium used different "resting-state" methodology (i.e., eyes open/close), we also studied a case–control-matched ABIDE subsample to avoid confounds arising from site-to-site differences. Specifically, we implemented a dissimilarity matrix procedure (Kaufman and Rousseeuw 1990) in R to create a case–control sample matching each ASD subject to an NT subject on the basis of age; this matching procedure was done within each site. The case–control-matched sample included 491 ASD (15.4 ± 6.3 years old) and 491 NT (15.7 ± 6.3 years old; Supplementary Table S1) males.

### Image Preprocessing

Structural and functional MRI scans from all 2156 subjects were processed in the Biowulf cluster at NIH (https://hpc.nih.gov/). The

**Table 1.** Age, intelligence (FIQ), and head motion (FD) for the selected ASD and NT males across sites (main sample)

| Site | No. subjects | | Age (years) | | FIQ | | FD (mm) | |
|---|---|---|---|---|---|---|---|---|
| | NT | ASD | NT | ASD | NT | ASD | NT | ASD |
| | | | Mean (SD) | | Mean (SD) | | Mean (SD) | |
| Caltech | 9 | 13 | 22 (3) | 25 (7) | 118 (8) | 104 (10) | 0.08 (0.03) | 0.09 (0.04) |
| CMU | 9 | 9 | 24 (4) | 27 (6) | 111 (11) | 114 (13) | 0.13 (0.05) | 0.11 (0.03) |
| KKI | 113 | 45 | 10 (1) | 11 (2) | 112 (12) | 100 (16) | 0.09 (0.04) | 0.10 (0.05) |
| MaxMun | 15 | 6 | 24 (6) | 20 (8) | 111 (11) | 105 (16) | 0.08 (0.03) | 0.06 (0.03) |
| Pittsburgh | 21 | 18 | 20 (6) | 19 (7) | 110 (11) | 113 (13) | 0.12 (0.03) | 0.12 (0.03) |
| Trinity | 23 | 23 | 17 (4) | 17 (4) | 117 (10) | 109 (15) | 0.08 (0.02) | 0.10 (0.03) |
| UCLA | 38 | 47 | 12 (3) | 13 (2) | 117 (12) | 102 (12) | 0.09 (0.04) | 0.08 (0.04) |
| USM | 46 | 50 | 21 (6) | 22 (7) | 108 (11) | 101 (17) | 0.08 (0.03) | 0.08 (0.04) |
| Leuven | 29 | 21 | 20 (5) | 20 (5) | 108 (11) | 109 (12) | 0.09 (0.03) | 0.08 (0.02) |
| NYU | 87 | 111 | 15 (6) | 11 (6) | 113 (13) | 106 (17) | 0.07 (0.02) | 0.07 (0.03) |
| OHSU | 37 | 39 | 10 (2) | 12 (2) | 117 (12) | 107 (18) | 0.07 (0.03) | 0.08 (0.04) |
| Olin | 19 | 23 | 18 (3) | 18 (2) | 109 (19) | 107 (26) | 0.12 (0.04) | 0.10 (0.03) |
| SBL | 4 | 5 | 24 (1) | 29 (5) | 110 (6) | 104 (5) | 0.12 (0.04) | 0.13 (0.02) |
| SDSU | 34 | 32 | 14 (3) | 14 (3) | 116 (12) | 105 (16) | 0.06 (0.03) | 0.05 (0.02) |
| Stanford | 6 | 8 | 11 (2) | 10 (2) | 113 (15) | 120 (16) | 0.05 (0.02) | 0.07 (0.02) |
| Yale | 13 | 9 | 13 (3) | 13 (4) | 114 (15) | 99 (33) | 0.07 (0.03) | 0.07 (0.02) |
| BNI | 9 | 12 | 20 (2) | 22 (6) | 109 (6) | 102 (12) | 0.14 (0.05) | 0.14 (0.04) |
| EMC | 14 | 14 | 8 (1) | 9 (1) | 113 (9) | 106 (0) | 0.08 (0.04) | 0.07 (0.03) |
| ETH | 22 | 7 | 24 (5) | 22 (4) | 113 (11) | 110 (14) | 0.09 (0.04) | 0.10 (0.04) |
| GU | 25 | 32 | 11 (2) | 11 (2) | 112 (7) | 120 (13) | 0.07 (0.03) | 0.09 (0.04) |
| IP | 7 | 13 | 21(5) | 16 (5) | 111 (15) | 93 (25) | 0.06 (0.05) | 0.08 (0.04) |
| IU | 13 | 15 | 23 (3) | 22 (5) | 116 (14) | 115 (13) | 0.09 (0.03) | 0.08 (0.04) |
| UCD | 9 | 13 | 15 (2) | 15 (2) | 126 (9) | 105 (13) | 0.08 (0.05) | 0.08 (0.04) |
| Totals | 602 | 565 | 15.3 (6.4) | 15.5 (6.8) | 113 (12) | 106 (16)* | 0.08 (0.04) | 0.08 (0.04) |

SD, standard deviation; FD: temporal mean of the framewise displacement; CMU: Carnegie Mellon Univ.; KKI: Kennedy Krieger Inst.; MaxMun: Maximilians Univ. (Munich); Trinity: Center for Health Sciences; Leuven Univ. (Belgium); Olin: Olin Inst of living (Hartford H); SBL: Social Brain Lab (Netherlands); USM: Utah Univ.; BNI: Barrow Neurol. Inst.; EMC: Erasmus Univ. (Rotterdam); ETH Zurich; GU: Georgetown Univ.; IP: Pasteur I. (France); IU: Indiana Univ.; UCD: University of California Davis.
*ASD < NT: $P < 0.05$

FreeSurfer (version 5.3.0) software package (http://surfer.nmr.mgh.harvard.edu) (Fischl et al. 2002) was used to automatically segment anatomical MRI scans into cortical and subcortical GM structures. The University of Oxford's Center for Functional Magnetic Resonance Imaging of the Brain (FMRIB) Software Library (FSL version 5.0; http://www.fmrib.ox.ac.uk/fsl) was used for image realignment (to correct for head motion with MCFLIRT, Motion Correction using FMRIB's Linear Image Registration Tool) and for spatial normalization to the MNI152 template using 3-mm isotropic voxels (with FLIRT, the FMRIB's Linear Image Registration Tool) (Jenkinson et al. 2002; Smith et al. 2004). All subsequent calculations (Fig. 1) were carried using the interactive data language (IDL, ITT Visual Information Solutions, Boulder, CO).

## Head Motion, Cerebrospinal Fluid, and WM Confounds

FD was computed for every time point from head translations and rotations. A 50-mm radius was used to convert angle rotations to displacements. Scrubbing was used to remove time points excessively contaminated with motion. Specifically, time points were excluded if the root-mean-squared change of the blood oxygenation level-dependent (BOLD) signal from volume to volume was larger than 0.5% and FD > 0.5 mm (Power et al. 2012). The number of time points removed per time series by scrubbing was not significantly different for ASD (1.1 ± 1.8; mean ± SD) than for NT males (1.0 ± 1.8; $P = 0.34$, t-test, 2-tailed).

Residual motion-related signal fluctuations were removed with multilinear regression using the 6-motion realignment parameters as regressors (Tomasi and Volkow 2010). Unwanted baseline drifts and high-frequency (respiratory and cardiac) components in the MRI signal were attenuated usingft 0.01–0.1 Hz band-pass filtering. The first 4 time points of the rfMRI time series were removed to avoid non-equilibrium effects in the BOLD signal. Two additional image-preprocessing pipelines were implemented for the removal of nuisance signals that showed temporal correlation with the average signal in cerebrospinal fluid (CSF) and WM regions (computed using the freesurfer parcellations) and the whole-brain average signal (i.e., global signal regression; GSR) (Tomasi and Volkow 2010).

## Functional Connectivity Density Mapping

We computed the number of local connections at every voxel location, that is, the number of elements in the local FC cluster, using a "growing" algorithm written in IDL (Tomasi and Volkow 2010). The Pearson correlation was used to assess the strength of the FC, $R_{ij}$, between voxels $i$ and $j$ in the brain. A previously optimized correlation threshold $R_{ij} > 0.6$ (Tomasi and Volkow 2010, 2011a, 2011b, 2011c, 2011d) was selected to ensure that significant correlations between time-varying signal fluctuations are corrected at $P_{FWE} < 0.05$. A voxel ($x_j$) was added to the list of voxels functionally connected with $\times_0$ only if it was adjacent to a voxel that was linked to $\times_0$ by a continuous path of functionally connected voxels and $R_{0j} > 0.6$. This calculation was repeated for all brain voxels that were adjacent to those that belonged to the list of voxel functionally connected to $\times_0$ in an iterative manner until no new voxels could be added to the list. Approximately, the procedure above captures degree

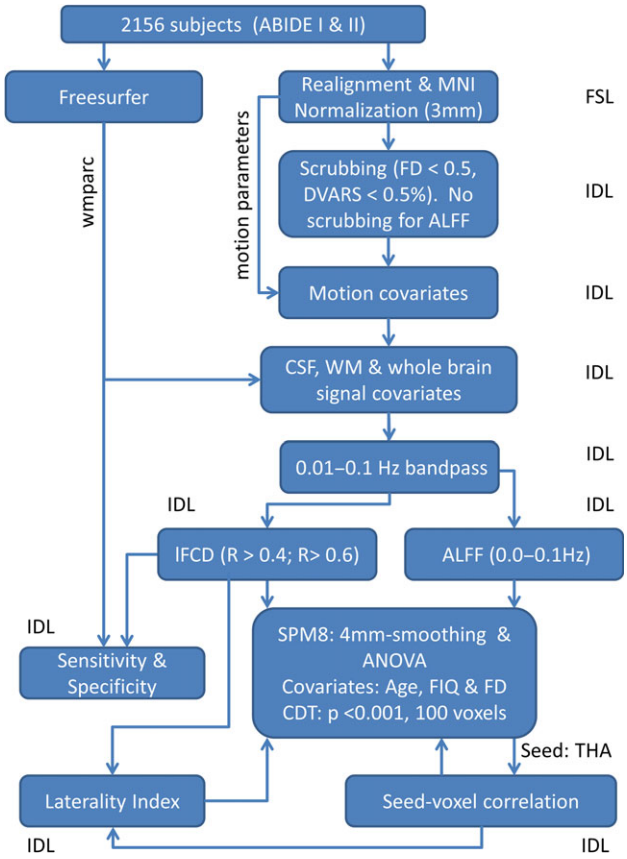


**Figure 1.** Image-processing pipelines. lFCD, ALFF, and FC maps with 3-mm isotropic resolution were computed for 656 ASD and 835 NT subjects from the ABIDE I and II image datasets (see text).

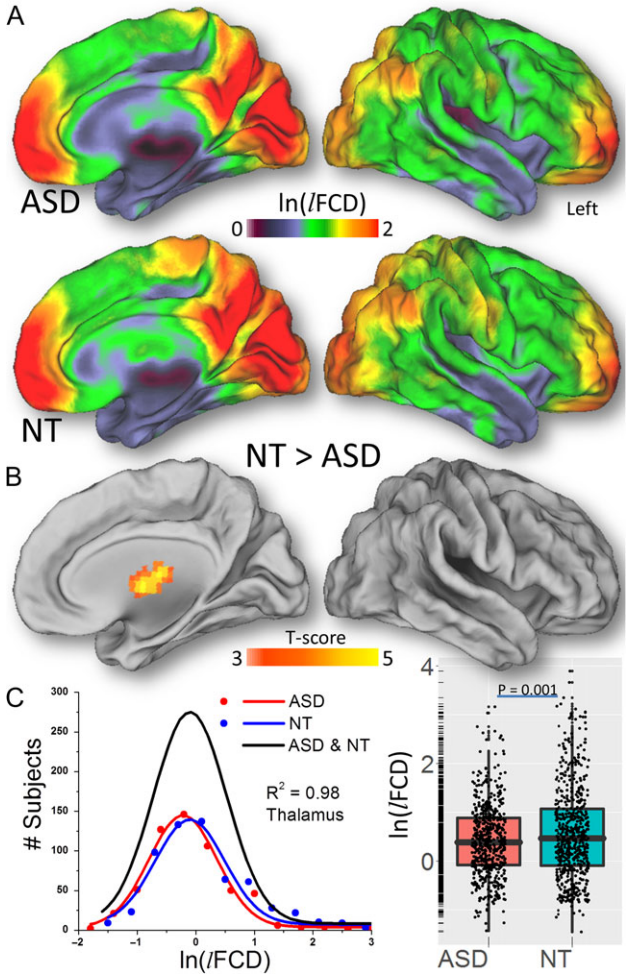


**Figure 2.** A Distribution of the lFCD hubs in the human brain for 565 ASD males and 602 NT males and their statistical differences (*B*) superimposed on medial and dorsal surface views of the population average atlas (PALS-B12) of the cerebral cortex. Frequency count for the logarithm of lFCD in the anterior thalamus across ASD (red) and NT (blue) males and the corresponding Gaussian curves that fit the data (*C*, left); the black Gaussian curve corresponds to all subjects. The logarithm of lFCD averaged across voxels in the whole thalamus, for ASD and NT (*C*, right). Image preprocessing includes WM and CSF signal covariates. lFCD was computed using a correlation threshold = 0.6.

(Rubinov and Sporns 2010) within 1-cm spherical volumes. Additionally, the lFCD was computed using a lower correlation threshold ($R > 0.4$) to assess the robustness of the findings to changes in the lFCD correlation threshold.

Grand mean scaling was implemented for each of the pipelines to reduce the variability of the lFCD associated with MRI technology differences across research sites and to normalize its distribution (Tomasi and Volkow 2010). Since the sensitivity to signal fluctuations and the Pearson correlation factors increase with signal-to-noise ratio (SNR) (DeDora et al. 2016), we assumed a linear approximation in which, like for the BOLD SNR, lFCD can be expressed as a product of independent factors for repetition time (TR), echo time (TE), voxel size, and coil/scanner/sequence (Craddock et al. 2013). These factors would be common to all subjects' rfMRI data collected by a research site, assuming that the MRI technology of the site was kept constant across subjects. Thus, a single scaling factor for each research site, $1/\langle lFCD \rangle$, reflecting the mean lFCD across subjects and voxels in the brain, would partially normalize the linear contributions of those variables to the lFCD across research sites. This procedure allowed us to merge lFCD datasets from different research sites, preserving the group differences in lFCD. Lastly, the logarithm of lFCD was computed to normalize the distribution of lFCD across subjects (Fig. 2A).

## Sensitivity and Specificity

Two benchmarks were used to quantify the quality of the lFCD: "sensitivity," a true positive rate that gauges the proportion of lFCD in GM, and "specificity," a true negative rate that gauges the proportion of WM voxels with lower lFCD than the whole-brain average (Tomasi et al. 2016a).

## Amplitude of the Spontaneous Signal Fluctuations (ALFF)

The preprocessed time series were also used to map the amplitude of low-frequency fluctuations (ALFF) for all voxels in the brain. Specifically, the fast Fourier transform was used to compute ALFF as the average of the power spectrum's square root in the 0.01–0.10 Hz frequency bandwidth (Yang et al. 2007).

## Seed–Voxel Correlations

The freesurfer partitions (wmparc) of the GM structures were also used to define seed regions corresponding to each individual subject for subsequent seed–voxel correlation analyses. Since the anterior thalamus demonstrated lower lFCD (i.e., local

**Table 2** Statistical significance, MNI coordinates, and volume for clusters showing group differences and/or age- and FIQ-related changes in lFCD and FC(THA)

| Region | BA | MNI coordinates [mm] | | | k | ASD > NT | Age | FIQ |
|---|---|---|---|---|---|---|---|---|
| | | x | y | z | Voxels | T | T | T |
| ln(lFCD) | | | | | | | | |
| Thalamus | N/A | −9 | −15 | 9 | 619 | −4.7 | 3.4 | NS |
| Thalamus | N/A | 15 | −15 | 12 | | −4.2 | NS | NS |
| Calcarine | 17 | 6 | −93 | −9 | 2570 | NS | 8.3 | NS |
| Angular | 39 | −45 | −72 | 33 | | NS | 6.6 | NS |
| Sup temporal | 22 | −60 | −12 | 0 | | NS | 6.5 | NS |
| Thalamus | N/A | 0 | −15 | 6 | 230 | −3.7 | 8.2 | −1.9 |
| Precentral | 6 | −45 | 6 | 48 | 1271 | NS | 7.0 | NS |
| Sup medial frontal | 10 | 0 | 57 | 6 | | NS | 6.5 | NS |
| Precentral | 6 | −42 | 0 | 54 | | NS | 6.5 | NS |
| Precentral | 6 | 48 | −9 | 54 | 464 | NS | 6.5 | NS |
| Precentral | 6 | 45 | 0 | 51 | | NS | 5.7 | NS |
| Middle frontal | 9 | 45 | 12 | 48 | | NS | 5.1 | NS |
| Middle cingulum | 24 | 3 | −6 | 45 | 252 | NS | 5.0 | NS |
| Paracentral lobule | 5 | 3 | −39 | 60 | | NS | 5.0 | NS |
| Post cingulate | 23 | −9 | −36 | 24 | 147 | NS | −9.9 | NS |
| Putamen/pallidum | N/A | 21 | 6 | 0 | 302 | NS | −8.5 | NS |
| Orbitofrontal | 11 | −33 | 60 | −15 | 240 | NS | −8.3 | NS |
| Putamen/pallidum | N/A | −27 | −6 | −3 | 160 | NS | −8.1 | NS |
| Orbitofrontal | 11 | 27 | 42 | −21 | 126 | NS | −7.6 | NS |
| Cerebellum | **4/5** | −24 | −45 | −21 | 153 | NS | NS | −4.8 |
| Cerebellum | 6 | −30 | −57 | −27 | | NS | NS | −3.9 |
| Cerebellum | **Crus1** | −33 | −72 | −30 | | NS | NS | −3.7 |
| Cerebellum | 3 | 15 | −36 | −21 | 240 | NS | NS | −4.7 |
| ParaHippocampal | 30 | −18 | −27 | −18 | | NS | NS | −4.2 |
| Lucus coeruleus | N/A | 6 | −30 | −12 | | NS | NS | −4.0 |
| Sup medial frontal | 32 | 12 | 48 | 27 | 132 | NS | NS | −4.2 |
| Superior frontal | 10 | 18 | 57 | 24 | | NS | NS | −4.0 |
| Sup medial frontal | 9 | 9 | 48 | 36 | | NS | NS | −3.8 |
| Thalamus | N/A | −3 | −6 | 6 | 123 | −4.1 | 5.2 | −3.8 |
| Thalamus | N/A | 0 | −21 | 9 | 0 | −3.3 | 3.7 | −3.6 |
| Thalamus | N/A | −15 | −6 | 3 | 0 | −3.3 | NS | −3.0 |
| FC(THA) | | | | | | | | |
| Middle temporal | 22 | −60 | −15 | −6 | 6688 | 6.3 | −7.3 | NS |
| Middle temporal | 21 | −63 | −27 | 3 | | 6.1 | −6.7 | NS |
| Postcentral | 3 | −51 | −24 | 54 | | 5.9 | −7.8 | NS |
| Middle cingulum | 6 | 3 | −12 | 51 | | 5.8 | −4.0 | NS |
| Suppl motor area | 6 | −6 | −18 | 63 | | 5.8 | −6.2 | NS |
| Postcentral | 4 | 51 | −18 | 42 | | 5.6 | −6.5 | NS |
| Insula | 48 | 36 | −27 | 18 | | 4.9 | −5.6 | NS |
| Middle temporal | 21 | 48 | −33 | −3 | | 4.9 | −5.3 | NS |
| Insula | 48 | 36 | −9 | 6 | | 4.8 | −9.0 | NS |

underconnectivity) for ASD than for NT, the whole thalamic partition from freesurfer was used as a seed region for subsequent seed–voxel correlation analyses. To assess the regional specificity of the findings, the cluster of voxels showing a significant difference in lFCD between ASD and NT was also used as a seed region for additional seed–voxel correlation analyses. The Pearson correlation between the time-varying signal of the seed and that of a given voxel was used to estimate the FC of the brain voxels with the thalamus seed [FC(THA)]. The Fisher transform was used to normalize the step-distributed correlation coefficients.

## Laterality

We assessed the laterality of the lFCD and thalamic FC maps using a voxelwise approach (Tomasi and Volkow 2012c). Briefly, maps with neurological convention (R: right is right) were additionally created by flipping the radiological maps (L) along the x-axis. Then, the strength of the right–left asymmetries was mapped voxel-by-voxel by using a laterality index, LI = (R − L) / (R + L) (Steinmetz 1996). Negative LI values indicate leftward asymmetry and positive LI values indicate rightward asymmetry. The Fisher transform was used to normalize the step-distributed LI values.

## Statistical Analyses

The metrics (lFCD, LI, ALFF, and seed–voxel correlation maps) were spatially smoothed with a 4-mm Gaussian kernel using the statistical parametric mapping software (SPM8; Wellcome Department of Cognitive Neurology, London, UK). One-way analysis of variance (ANOVA) with age, FIQ, and FD covariates was implemented in

SPM8 to map group differences and the effects of age, FIQ, and FD, independently for each metric and pipeline. Statistical significance was set as $P_{FWE} < 0.05$, corrected for multiple comparisons at the cluster level with a family-wise error (FWE) correction on the basis of the SPM Gaussian random field theory. Unless otherwise specified in the text, a cluster-defining threshold, $P < 0.001$, and a minimum cluster size of 100 voxels were used in the corrections for multiple comparisons, following current reporting standards (Eklund et al. 2016). Brain regions were labeled according to the Automated Anatomical Labeling atlas and the Brodmann atlas, which are included in the MRIcro software (http://people.cas.sc.edu/rorden/mricron/index.html).

## Results

Head motion was not significantly larger for ASD males (⟨FD⟩ = 0.084 ± 0.037 mm; mean ± standard deviation) than for NT males (⟨FD⟩ = 0.083 ± 0.037 mm; $P > 0.45$, *t*-test; Table 1). There were no significant differences in ALFF between ASD males and NT males in any brain region ($P_{FWE} > 0.05$, FWE-corrected for multiple comparisons). GM sensitivity (NT: 53 ± 6%; ASD: 54 ± 6%) and specificity (NT: 83 ± 5%; ASD: 84 ± 5%) of the lFCD did not differ between male groups ($P > 0.6$, 2-tailed).

The lFCD computed with the GSR procedure led to spurious lFCD in WM and CSF, compared with lFCD computed without nuisance signal regression (either whole brain or from WM and CSF), ($P_{FWE} < 0.0001$, corrected for multiple comparisons in the whole brain), consistent with our previous studies (Tomasi et al. 2016a). The regression of signals in WM and CSF reduced the lFCD in precuneus, occipital, medial prefrontal, and cingulate cortices and in the thalamus ($P_{FWE} < 0.0001$). Since nuisance signal regression did not alter the lFCD differences between the ASD and NT male groups in any brain region ($P_{FWE} > 0.05$), here we report results for lFCD datasets computed after removal of signal fluctuations arising from WM and CSF.

Similarly, there was no significant difference in any brain region between lFCD datasets computed using high ($R > 0.6$) versus those computed using low ($R > 0.4$) correlation thresholds ($P_{FWE} > 0.05$). Since the selection of the threshold did not alter significantly, the lFCD differences between ASD and NT male groups in any brain region ($P_{FWE} > 0.05$), here we report results using the most conservative approach ($R > 0.6$). All statistical findings below were reproduced in the case–control-matched sample (see Supplementary Material).

### lFCD: Patterns

The average distribution of the lFCD across males was highly symmetrical and similar for NT and ASD (Fig. 2A). Specifically, the lFCD was high ($1.3 < \ln(\text{lFCD}) < 2$) in the occipital cortex, superior and inferior parietal lobes, and default mode network regions (precuneus, angular gyrus, and the medial orbitofrontal and superior frontal cortex). The lFCD was moderate ($0.7 < \ln(\text{lFCD}) < 1.3$) in the postcentral and precentral gyri, middle and anterior cingulate, lateral occipital, dorsolateral and inferior frontal cortices, and the posterior lobe of the cerebellum. The lFCD was low ($\ln(\text{lFCD}) < 0.7$) in the thalamus, basal ganglia, superior and medial temporal cortices, temporal pole, insula, midbrain, pons, and the anterior lobe of the cerebellum (Fig. 2A).

### lFCD: Group Difference

Compared with the NT male group, the only brain region where the ASD male group had lower lFCD was in anterior thalamus (left and right, including ventral anterior and dorsomedial nuclei) after whole-brain corrections for multiple comparisons ($P_{FWE} < 0.005$, Fig. 2B, Table 2; effect size: $0.09 < r < 0.15$, df = 1162). Fig. 2C demonstrates the normal distribution of the average ln(lFCD) in the anterior thalamus across subjects (left panel), which was lower for ASD than for NT males (right panel). There was no brain region where ASD males had significantly greater lFCD than NT males. Group differences in thalamic ln(lFCD) between ASD and NT were not statistically significant in females ($P = 0.55$).

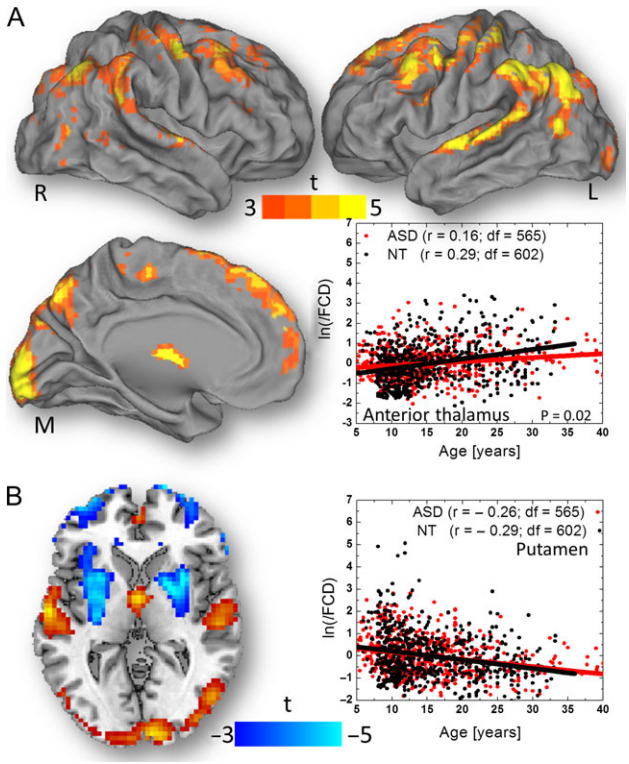


**Figure 3.** Statistical significance of age-related increases in lFCD across 565 ASD and 602 NT males (conjunction contrast) rendered on medial (M), left (L), and right (R) surface views of the PALS-B12 atlas. The scatter plot (A, right) demonstrates the age-related lFCD increases in the anterior thalamus for ASD (*r* is the Pearson correlation between red data points and regression line) and for NT (black data points and regression line) and the group differences in the regression slope ($P = 0.02$). Statistical significance of age-related effects on lFCD across all subjects superimposed on an axial view of the brain (B, left). The age-related decreases of lFCD were maximal in bilateral putamen and did not show significant age-by-group interaction effects (B, right).

### Age

Fig. 3A and Table 2 show that in males, brain maturation from 5 years to 40 years of age was associated with increased lFCD in several brain regions, comprising anterior and medial thalamus, primary visual cortex (BA 17), middle and posterior cingulum (BA 23 and 24), angular gyrus (BA 39), superior temporal (BA 22), paracentral lobule (BA 5), precentral (BA 6), and medial, middle, and superior frontal (BAs 6, 9, and 10) gyri. The age-related lFCD increases in the anterior thalamus, anterior cerebellar lobe, calcarine cortex, superior temporal gyrus, orbitofrontal cortex, and left pars triangularis ($P_{FWE} < 0.001$; $0.10 < r < 0.25$, $df = 1162$) were more pronounced for the left than for the right brain hemisphere, and for NT than for ASD males. The scatter

plot in Fig. 3A exemplifies the linear increases in lFCD with age in the thalamus ROI, which were steeper for NT than for ASD males ($P = 0.02$). Conversely, in posterior cingulum, putamen, and orbitofrontal cortex, the lFCD decreased with age ($P_{FWE} < 0.001$; Fig. 3 and Table 2; effect size: $0.22 < r < 0.28$, $df = 1162$). The slope of the age-related lFCD decreases in these regions, however did not differ between ASD and NT males.

## Laterality

Statistical analysis (ANOVA; conjunction NT and ASD) of the LI of the lFCD across all subjects revealed right-lateralization in inferior parietal cortex (BA 40), Rolandic operculum (BA 48), insula (BA 48), calcarine cortex (BA 17), supramarginal (BA 48), precentral (BA 6), middle and superior temporal (BAs 20, 21 and 41), and middle occipital (BA 18) and frontal (BA 46) gyri, and left-lateralization in medial orbitofrontal cortex (BA 10 and 11), anterior (BA 24) and posterior (BA 23) cingulum and precuneus (BA 31) ($P_{FWE} < 0.001$; Fig. 4). The trend toward a stronger right-lateralization of the lFCD in the inferior parietal cortex for the ASD than the NT male group did not reach significance ($P_{FWE} = 0.06$; Fig. 4).

## Associations With Clinical Outcomes

Linear regression analysis across subjects showed that the reduced lFCD in the whole thalamus was associated with increased ADOS total and with increased ADI-R social ($P < 0.007$; Fig. 5), such that the lower the lFCD in thalamus, the greater the severity of ASD symptoms and the greater the disruption in social behaviors.

## Seed–Voxel Correlations

Fig. 6A shows that the thalamus seed (Fig. 6C) had bilateral positive FC with the cingulum, amygdala, caudate, globus pallidus, putamen, ventral tegmental area, hippocampus, parahippocampal and superior temporal gyri, insula, pons (Fig. 6A), posterior lobe of cerebellum, vermis, and deep cerebellar nuclei (not shown). The negative FC of the thalamus was constrained to occipital regions (cuneus and lingual, fusiform, and superior and middle occipital gyri), and superior and inferior parietal cortices (Fig. 6A). Compared with the NT male group, ASD males had stronger thalamic FC, bilaterally, in the middle temporal gyrus, insula, middle cingulum, supplementary motor area, and in the postcentral gyrus ($P_{FWE} < 0.004$; Fig. 6B and Table 2; $0.14 < r < 0.18$, $df = 1162$).

As an example, Fig. 6D shows the normal distribution across subjects of the average FC between the thalamus (THA) and the middle temporal gyrus (MTG) and the stronger coupling between these regions for ASD than for NT male subjects. These regions also demonstrated significant age-related decreases in FC with thalamus ($P_{FWE} < 0.001$; Fig. 6E and F). Neither the age-related decreases of FC(THA) nor its LI index differs significantly for ASD and NT males. Comparable findings emerged from the anterior thalamic seed ($P_{FWE} < 0.004$; Fig. S2).

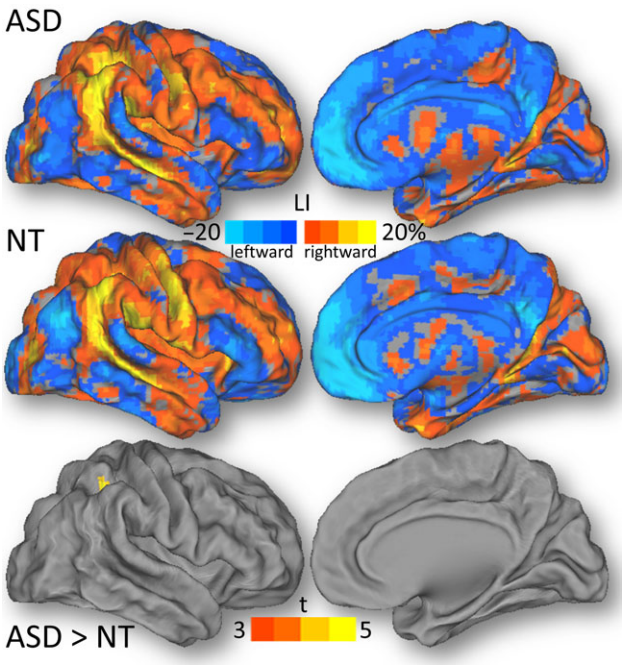


Figure 4. The LI, averaged across 565 ASD males and 602 NT males, and the statistical group differences, rendered on dorsal (D) and medial (M) surface views, of the PALS-B12 atlas.

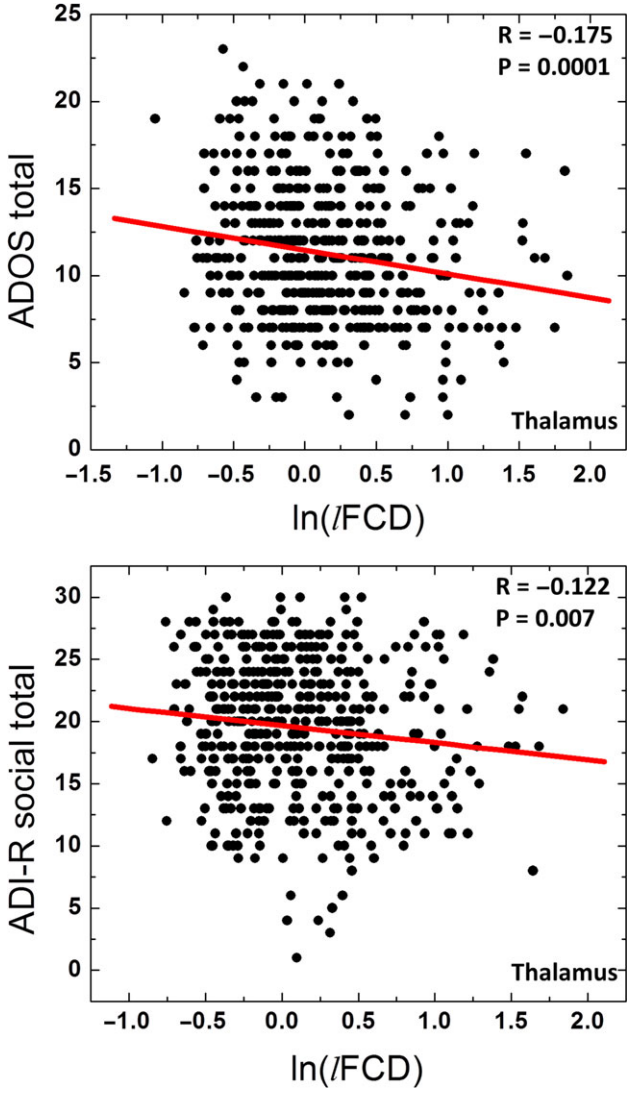


Figure 5. Scatter plots showing the linear association across ASD participants ($N = 491$ for ADOS total and 478 for ADI-R social) between the average ln(lFCD) in the whole thalamus and "gold standard" metrics in the diagnosis of ASD.

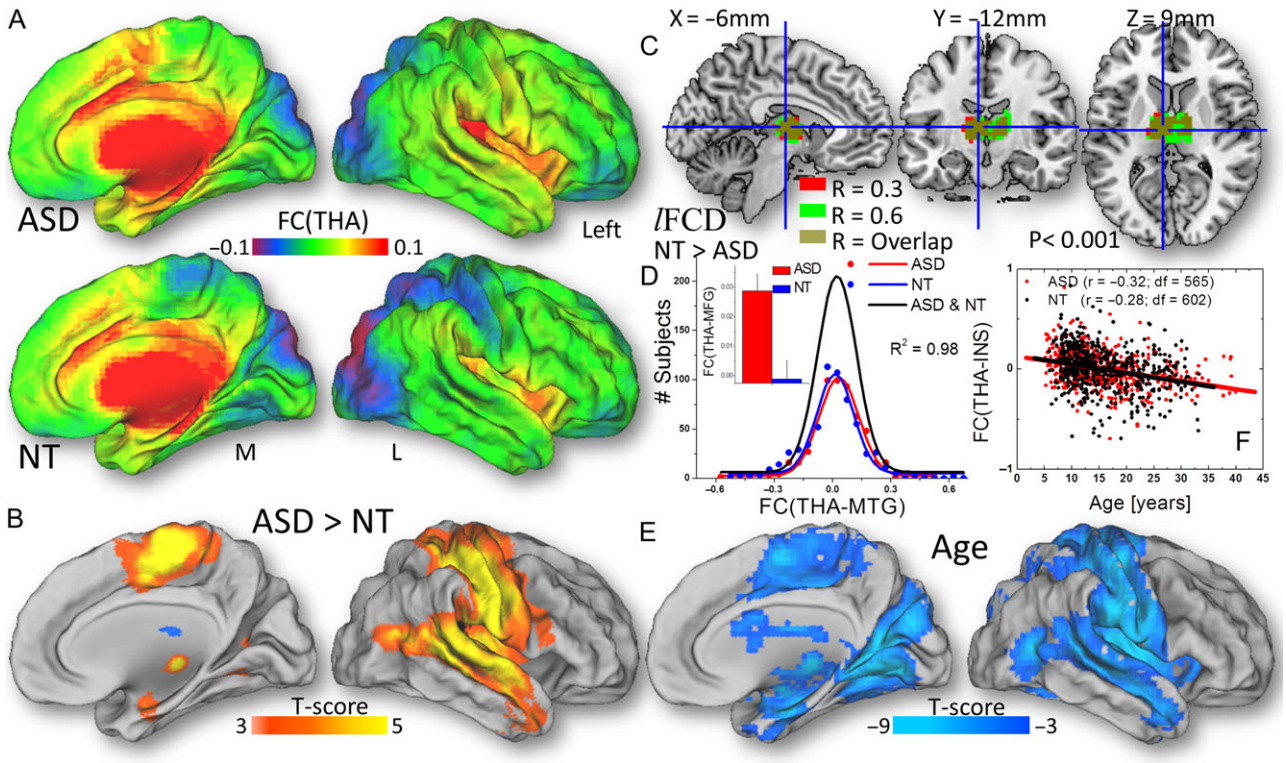


**Figure 6.** The strength of the FC of the thalamus (THA) seed across 565 ASD males and 602 NT males (*A*) and their statistical differences (*B*), superimposed on the medial (M) and dorsal (L) views of the PALS-B12 atlas. *C*: Thalamus seed used for seed–voxel correlation analysis, overlaid on 3 orthogonal views of the brain. *D*: Frequency count for the strength of the FC of the thalamus seed for ASD (red) and for NT (blue) males and the corresponding Gaussian curves that fit the data; the black Gaussian curve corresponds to all subjects. The bar plot insert exemplifies the group differences in FC between the thalamus (THA) and the medial temporal gyrus (MTG) ($P < 0.001$). *E*: Statistical significance of age-related decreases in the FC of the thalamus. *F*: The scatter plot illustrates the age-related decreases in the FC between the thalamus and the insula, which did not differ significantly between ASD (red) and NT (black).

The connectivity of the anterior thalamus did not differ significantly from that of the whole thalamus in any brain region.

Similar group differences on thalamic connectivity were found for females using a region-of-interest approach, which covered most clusters in Table 2. Specifically, FC(THA) was averaged independently within 5 bilateral anatomical partitions of the MRI structure (postcentral, precentral, and middle temporal gyri, insula, and the banks of the superior temporal sulcus; from freesurfer's wmparc) for each individual subject (Fig. 7A). Similar to males, ASD females exhibited hyperthalamic connectivity in postcentral, precentral, and middle temporal gyri, insula, and the banks of the superior temporal sulcus ($P < 0.006$) compared with NT females (Fig. 7B). Except for the middle temporal gyrus, these regions also demonstrated age-related decreases in FC(THA) in females ($R < -0.17$; $P < 0.002$). In the banks of the superior temporal sulcus, middle temporal, precentral, and postcentral gyri, the age-related decreases of thalamic connectivity were blunted in ASD females compared with NT females ($P < 0.04$, 1-tailed; Fig. 7C).

## DISCUSSION

The underconnectivity hypothesis proposes a disruption of complex information processing in ASD (Belmonte et al. 2004; Just et al. 2004), a premise that has found inconsistent support during the last decade (Müller et al. 2011), perhaps due to the heterogeneity of ASD (Masi et al. 2017), combined with the small study samples and the lack of adequate methodology to measure local connectivity. Here, we take advantage of unusually large samples of 565 ASD and 602 NT males and of 91 ASD and 233 NT females to assess local connectivity in the brain using data-driven lFCD, and long-range connectivity using seed–voxel correlations. Contrary to the original hypothesis, we observed local underconnectivity in anterior thalamus and increased long-range connectivity of the thalamus with auditory, somatosensory, motoric, and interoceptive (insula) cortices and with parietal regions.

The thalamus, a subcortical–cortical relay that until recently had been mostly ignored by MRI studies on autism (Schuetze et al. 2016), demonstrated the most striking of the FC abnormalities. In particular, the anterior thalamus, which encompasses the ventral anterior and dorsomedial nuclei that project to the prefrontal cortex and to primary/association visual, auditory, and somatosensory cortical areas (Behrens et al. 2003), demonstrated lower lFCD for ASD than for NT. This region also showed increases in lFCD with aging that were more pronounced for NT than for ASD. A negative association between age and the long-range connectivity of the thalamus emerged from seed–voxel correlations in lateral cortical regions that show thalamic overconnectivity in ASD compared with NT. Importantly, reduced lFCD in the thalamus was associated with increasing symptoms of autism such that ASD subjects with increasing ADOS total and ADI-R social scores had decreased local connectivity in the thalamus. We had previously shown that regional lFCD correlates with regional brain glucose metabolism, which serves as a marker of brain activity (Tomasi et al. 2013), and suggested that reduced lFCD might reflect disrupted neuronal thalamic activity. Indeed, using magnetic resonance spectroscopy (MRS), a recent study reported decreased *N*-acetyl

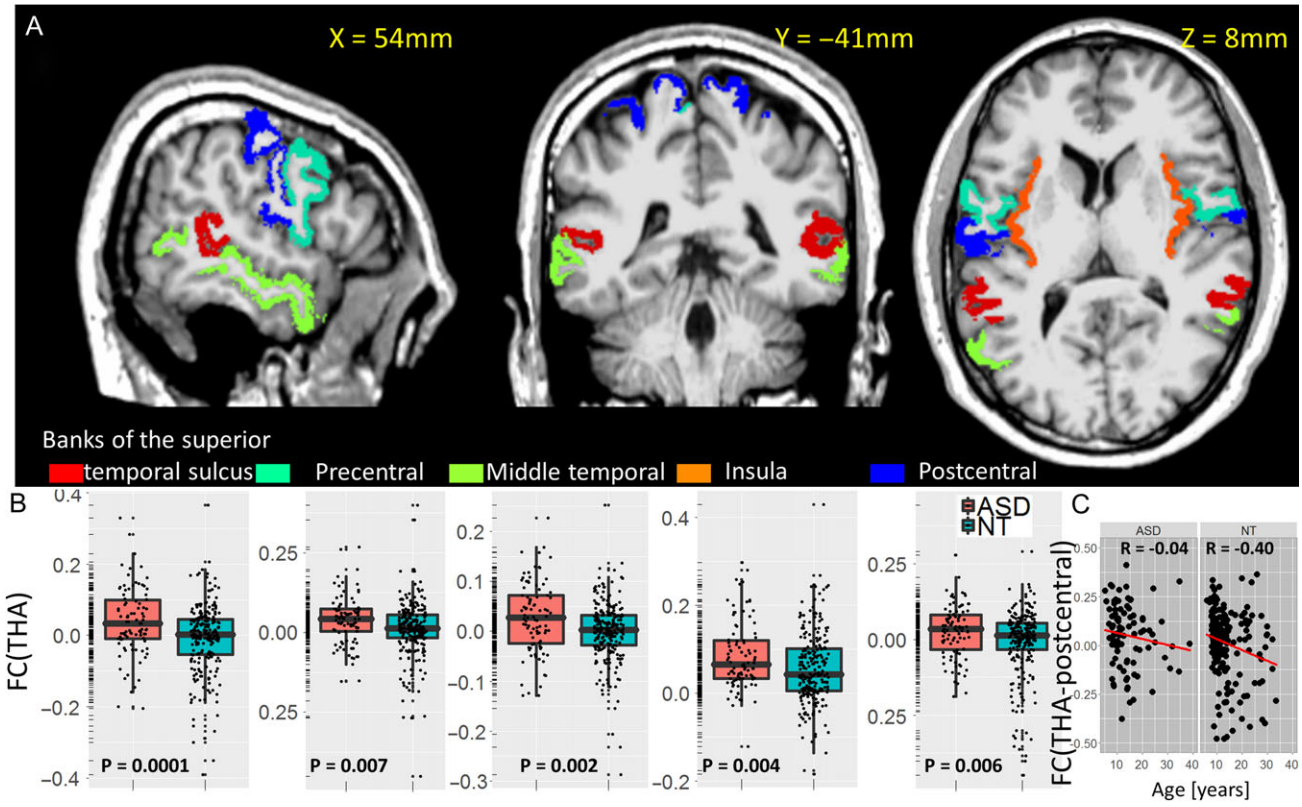


**Figure 7.** A Anatomical ROIs in which the strength of the FC of the thalamus (THA) seed differ between 91 ASD females and 233 NT females (*B*), superimposed on 3 orthogonal views of the human brain in the MNI space. C: Scatter plots illustrate the age-related decreases in FC(THA), which differ significantly between ASD and NT females.

aspartate (NAA), which is a marker of neuronal integrity, in the thalamus of 47 ASD, which as for our study was associated with greater ASD symptom severity (Hegarty et al. 2018). Also a study using positron emission tomography and 18 F-fludeoxyglucose reported reduced glucose metabolism in the thalamus of 17 ASD individuals (Haznedar et al. 2006). Thus, our findings are consistent with a slower maturation of short-range thalamic connectivity and long-range thalamo-cortical connectivity in ASD that disrupts thalamic activity and might contribute to symptom severity in ASD.

The thalamus had higher FC with insula, somatosensory, motor, premotor, and auditory areas and the middle cingulum, which are brain regions involved in the neuroanatomy of social cognition (Adolphs 2001), for ASD than for NT. This hyperconnectivity did not differ between the anterior seed and the whole-thalamus seed, suggesting that the effects were not specific to the anterior thalamus. Postmortem studies have associated some of these regions with the 3 core set of behaviors that are impaired in autism: social (superior temporal sulcus), language and communication (thalamus, superior temporal sulcus, and premotor cortex), and repetitive and stereotyped behaviors (thalamus)(Amaral et al. 2008).

All of these regions showed age-related reductions in FC with the thalamus in both groups, consistent with the emergence of aging effects on the FC of the nigro-thalamo-cortical pathway (Tomasi and Volkow 2014a). Our findings of increased long-range thalamo-cortical connectivity are consistent with prior findings reporting differences in thalamic connectivity between 79 ASD and 105 NT subjects of the ABIDE I sample (Baldwin et al. 2016), increased subcortical–cortical connectivity in 166 ASD subjects (Cerliani et al. 2015), increased thalamic connectivity in the right temporal lobe in 26 ASD children (Nair et al. 2013) and in temporal and parietal cortices in 228 ASD subjects (Woodward et al. 2017), and with increased connectivity between subcortical (thalamus and globus pallidus) and primary sensorimotor regions from the ABIDE I sample (Di Martino et al. 2014). Additionally, a recent study that evaluated thalamo-cortical FC reported thalamic overconnectivity, predominantly with limbic and sensorimotor regions (except for amygdala and occipital cortex), and underconnectivity with association cortices in 37 ASD children (Nair et al. 2015). Our results are also consistent with findings of morphological abnormalities in the shape and surface area of the thalamus (Tsatsanis et al. 2003; Schuetze et al. 2016) and with FC abnormalities of the thalamus (Nair et al. 2013; Schuetze et al. 2016) in ASD. However, additional systematic studies are needed to link the FC of the thalamus to its morphology. Intriguingly, a recent study reported reduced dynamics of resting network activity in adults with ASD (Watanabe and Rees 2017). To the extent that the thalamus plays a critical role in orchestrating information flow throughout cortical networks (Sherman and Guillery 2011; Bell and Shine 2016), one could hypothesize that disruptions in thalamic connectivity could underlie the overly stable neural dynamics observed in adults with ASD (Watanabe and Rees 2017).

Genetic (Eapen 2011), developmental (Baron-Cohen et al. 1985), and environmental (Risch et al. 2014) factors have been implicated in the abnormal growth and maturation of the autistic brain. Specifically, recent studies implicate genes involved in brain development such as those needed for axonal and dendritic growth and synaptogenesis (Toro et al. 2010; Hussman et al.

2011). Developmental anomalies in fetal and postnatal brain development, with early overgrowth (Courchesne et al. 2011) followed by a subsequently stunting in brain growth (Courchesne et al. 2011), are implicated in the aberrant cortical organization and connectivity of the autistic brain. Environmental factors during pregnancy could also interfere with the normal development of the fetal brain in ASD (Lyall et al. 2016).

Our results in ASD provide evidence of local underconnectivity at the macroscopic level in the anterior thalamus and of aberrant long-range thalamic connectivity characterized by a higher connectivity of the thalamus with auditory, somatosensory, premotor, and interoceptive and parietal regions. This disrupted pattern of thalamic connectivity in ASD is reminiscent to the one we observed in schizophrenia (Tomasi and Volkow 2014b). Although ASD and schizophrenia are distinct disorders, studies have pointed to the convergence in their neurobiology (imbalance in excitation/inhibition signaling involving glutamatergic and GABAergic circuit dysfunction) and clinical presentation (social dysfunction, sensory abnormalities)(Foss-Feig et al. 2017). Thus, our findings of thalamic local underconnectivity and disrupted thalamic long-range connectivity in ASD identify another neurobiological convergence between ASD and schizophrenia.

The group effects we detected are relatively small. Note that we were unable to reproduce the findings for any of the isolated 23 sites in the ABIDE dataset, which reflects the small size of the effects and highlights the importance of data-sharing initiatives such as ABIDE for detecting subtle effects in neuroimaging studies. We studied the left–right symmetry of the FC metrics in ASD and NT because core language areas that are essential for social communication showed left-lateralization in FC (Tomasi and Volkow 2012d), and atypical brain lateralization could be one cause of disordered language development in autism (Herbert et al. 2005). Despite our large sample size, we did not detect pronounced laterality differences in lFCD or FC (THA) metrics between the groups, which is inconsistent with the lateralization of the FC of language (Nielsen et al. 2014), motor, and premotor areas (Carper et al. 2015; Floris et al. 2016) that has been reported in ASD.

In our study, we corroborated the findings of long-range thalamic hyperconnectivity in ASD females that we observed in the male ASD group. However, we did not observe differences on local thalamic connectivity in the female ASD group. Although this could reflect the much smaller sample of female individuals with ASD than for the male cohort, we cannot rule out the possibility that they could reflect sex differences in neuropathology.

The voxelwise lFCD and thalamic FC metrics are based on spontaneous low-frequency fluctuations (0–0.1 Hz) in the BOLD-fMRI signal. Like in fMRI, the macroscopic resting-state signals result from numerous cells (in the cortex, 3-mm isotropic voxels contain ~7E+04 neurons and ~25E+04 glial cells (Lent et al. 2012)) and vessels can be affected by vascular confounds limiting the interpretability of the results. Thus, our finding of local underconnectivity in the thalamus does not negate the possibility that there might be microscopic overconnectivity in ASD. Although histological studies in postmortem brains of individuals with ASD have reported evidence consistent with increased synaptic neuronal connectivity in cortical brain regions (Hutsler and Zhang 2010; Zikopoulos and Barbas 2010), an immunohistological study reported reduced levels of alpha7 and beta2 nicotinic receptor subunits in the thalamus, consistent with neuronal loss in ASD (Ray et al. 2005). Although we are interpreting the decreased thalamic lFCD to reflect reduced neuronal thalamic connectivity, we cannot rule out the possibility that increased synaptic neurocircuitry might interfere with signaling between local thalamic neuronal microcircuits resulting in reduced lFCD.

Our findings in the context of prior results provide strong evidence of disrupted long-range thalamo-cortical connectivity in ASD that is consistent with delayed developmental maturation. They also implicate the thalamus as a key region in the neuropathology of ASD that might contribute to deficits in social communication, sensory processing, and repetitive motor behaviors in ASD.

## Supplementary Material

Supplementary material is available at *Cerebral Cortex* online.

## Funding

This work, accomplished with support from the National Institute on Alcohol Abuse and Alcoholism (Y1AA-3009), utilized the Biowulf cluster of the High-Performance Computing at the National Institutes of Health (http://hpc.nih.gov).

## Notes

*Conflict of Interest*: None declared.

## References

Abrams D, Lynch C, Cheng K, Phillips J, Supekar K, Ryali S, Uddin L, Menon V. 2013. Underconnectivity between voice-selective cortex and reward circuitry in children with autism. Proc Natl Acad Sci USA. 110:12060–12065.

Adolphs R. 2001. The neurobiology of social cognition. Curr Opp Neurobiol. 11:231–239.

Alaerts K, Woolley D, Steyaert J, Di Martino A, Swinnen S, Wenderoth N. 2014. Underconnectivity of the superior temporal sulcus predicts emotion recognition deficits in autism. Soc Cogn Affect Neurosci. 9:1589–1600.

Amaral D, Schumann C, Nordahl C. 2008. Neuroanatomy of autism. Trends Neurosci. 31:137–145.

Anderson J, Druzgal T, Froehlich A, Dubray M, Lange N, Alexander A, Abildskov T, Nielsen J, Cariello A, Cooperrider J, et al. 2011. Decreased interhemispheric functional connectivity in autism. Cereb Cortex. 21:1134–1146.

Assaf M, Jagannathan K, Calhoun V, Miller L, Stevens M, Sahl R, O'Boyle J, Schultz R, Pearlson G. 2010. Abnormal functional connectivity of default mode sub-networks in autism spectrum disorder patients. Neuroimage. 53:247–256.

Baldwin P, Curtis K, Patriquin M, Wolf V, Viswanath H, Shaw C, Sakai Y, Salas R. 2016. Identifying diagnostically-relevant resting state brain functional connectivity in the ventral posterior complex via genetic data mining in autism spectrum disorder. Autism Res. 9:553–562.

Baron-Cohen S, Leslie A, Frith U. 1985. Does the autistic child have a "theory of mind"? Cognition. 21:37–46.

Baxter A, Brugha T, Erskine H, Scheurer R, Vos T, Scott J. 2015. The epidemiology and global burden of autism spectrum disorders. Psychol Med. 45:601–613.

Behrens T, Johansen-Berg H, Woolrich M, Smith S, Wheeler-Kingshott C, Boulby P, Barker G, Sillery E, Sheehan K, Ciccarelli O, et al. 2003. Non-invasive mapping of connections between human thalamus and cortex using diffusion imaging. Nat Neurosci. 6:750–757.

Bell P, Shine J. 2016. Subcortical contributions to large-scale network communication. Neurosci Biobehav Rev. 71:313–322.

Belmonte M, Allen G, Beckel-Mitchener A, Boulanger L, Carper R, Webb S. 2004. Autism and abnormal development of brain connectivity. J Neurosci. 24:9228–9231.

Carper R, Solders S, Treiber J, Fishman I, Müller R. 2015. Corticospinal tract anatomy and functional connectivity of primary motor cortex in autism. J Am Acad Child Adolesc Psychiatry. 54:859–867.

Cerliani L, Mennes M, Thomas R, Di Martino A, Thioux M, Keysers C. 2015. Increased functional connectivity between subcortical and cortical resting-state networks in autism spectrum disorder. JAMA. Psychiatry. 72:767–777.

Cherkassky V, Kana R, Keller T, Just M. 2006. Functional connectivity in a baseline resting-state network in autism. Neuroreport. 17:1687–1690.

Courchesne E, Campbell K, Solso S. 2011a. Brain growth across the life span in autism: age-specific changes in anatomical pathology. Brain Res. 1380:138–145.

Courchesne E, Mouton P, Calhoun M, Semendeferi K, Ahrens-Barbeau C, Hallet M, Barnes C, Pierce K. 2011b. Neuron number and size in prefrontal cortex of children with autism. JAMA. 306:2001–2010.

Craddock R, Jbabdi S, Yan C, Vogelstein J, Castellanos F, Di Martino A, Kelly C, Heberlein K, Colcombe S, Milham M. 2013. Imaging human connectomes at the macroscale. Nature Methods. 10:524–539.

Dajani D, Uddin L. 2016. Local brain connectivity across development in autism spectrum disorder: a cross-sectional investigation. Autism Res. 9:43–54.

DeDora D, Nedic S, Katti P, Arnab S, Wald L, Takahashi A, Van Dijk K, Strey H, Mujica-Parodi L. 2016. Signal fluctuation sensitivity: an improved metric for optimizing detection of resting-state fMRI networks. Frontiers in Neuroscience. 10:180.

Di Martino A, Kelly C, Grzadzinski R, Zuo X, Mennes M, Mairena M, Lord C, Castellanos F, Milham M. 2011. Aberrant striatal functional connectivity in children with autism. Biol Psychiatry. 69:847–856.

Di Martino A, Yan C, Li Q, Denio E, Castellanos F, Alaerts K, Anderson J, Assaf M, Bookheimer S, Dapretto M, et al. 2014. The autism brain imaging data exchange: towards a large-scale evaluation of the intrinsic brain architecture in autism. Mol Psychiatry. 19:659–667.

Doucet G, Naveau M, Petit L, Zago L, Crivello F, Jobard G, Delcroix N, Mellet E, Tzourio-Mazoyer N, Mazoyer B, et al. 2012. Patterns of hemodynamic low-frequency oscillations in the brain are modulated by the nature of free thought during rest. Neuroimage. 59:3194–3200.

Eapen V. 2011. Genetic basis of autism: is there a way forward? Curr Opin Psychiatry. 24:226–236.

Ebisch S, Gallese V, Willems R, Mantini D, Groen W, Romani G, Buitelaar J, Bekkering H. 2011. Altered intrinsic functional connectivity of anterior and posterior insula regions in high-functioning participants with autism spectrum disorder. Hum Brain Mapp. 32:1013–1028.

Ecker C, Schmeisser M, Loth E, Murphy D. 2017. Neuroanatomy and neuropathology of autism spectrum disorder in humans. Adv Anat Embryol Cell Bio. 224:27–48.

Eklund A, Nichols T, Knutsson H. 2016. Cluster failure: why fMRI inferences for spatial extent have inflated false-positive rates. Proc Natl Acad Sci USA. 113:7900–7905.

Fischl B, Salat D, Busa E, Albert M, Dieterich M, Haselgrove C, van der Kouwe A, Killiany R, Kennedy D, Klaveness S, et al. 2002. Whole brain segmentation: automated labeling of neuroanatomical structures in the human brain. Neuron. 33: 341–355.

Fishman I, Datko M, Cabrera Y, Carper R, Müller R. 2015. Reduced integration and differentiation of the imitation network in autism: a combined functional connectivity magnetic resonance imaging and diffusion-weighted imaging study. Ann Neurol. 78:958–969.

Floris D, Barber A, Nebel M, Martinelli M, Lai M, Crocetti D, Baron-Cohen S, Suckling J, Pekar J, Mostofsky S. 2016. Atypical lateralization of motor circuit functional connectivity in children with autism is associated with motor deficits. Mol Autism. 7:35.

Foss-Feig J, Adkinson B, Ji J, Yang G, Srihari V, McPartland J, Krystal J, Murray J, Anticevic A. 2017. Searching for cross-diagnostic convergence: neural mechanisms governing excitation and inhibition balance in schizophrenia and autism spectrum disorders. Biol Psychiatry. 81:848–861.

Frith U. 1989. Autism: explaining the enigma. Oxford: Blackwell Publishing.

Haznedar M, Buchsbaum M, Hazlett E, LiCalzi E, Cartwright C, Hollander E. 2006. Volumetric analysis and three-dimensional glucose metabolic mapping of the striatum and thalamus in patients with autism spectrum disorders. Am J Psychiatry. 163:1252–1263.

Hegarty JN, Gu M, Spielman D, Cleveland S, Hallmayer J, Lazzeroni L, Raman M, Frazier T, Phillips J, Reiss A, Hardan A. 2018. A proton MR spectroscopy study of the thalamus in twins with autism spectrum disorder. Prog Neuropsychopharmacol Biol Psychiatry. 81:153–160.

Herbert M, Ziegler D, Deutsch C, O'Brien L, Kennedy D, Filipek P, Bakardjiev A, Hodgson J, Takeoka M, Makris N, et al. 2005. Brain asymmetries in autism and developmental language disorder: a nested whole-brain analysis. Brain. 128:213–226.

Hussman J, Chung R, Griswold A, Jaworski J, Salyakina D, Ma D, Konidari I, Whitehead P, Vance J, Martin E, et al. 2011. A noise-reduction GWAS analysis implicates altered regulation of neurite outgrowth and guidance in autism. Mol Autism. 2:1.

Hutsler J, Zhang H. 2010. Increased dendritic spine densities on cortical projection neurons in autism spectrum disorders. Brain Res. 1309:83–94.

Itahashi T, Yamada T, Watanabe H, Nakamura M, Ohta H, Kanai C, Iwanami A, Kato N, Hashimoto R. 2015. Alterations of local spontaneous brain activity and connectivity in adults with high-functioning autism spectrum disorder. Mol Autism. 6:30.

Jenkinson M, Bannister P, Brady M, Smith S. 2002. Improved optimization for the robust and accurate linear registration and motion correction of brain images. Neuroimage. 17: 825–841.

Just M, Cherkassky V, Keller T, Minshew N. 2004. Cortical activation and synchronization during sentence comprehension in high-functioning autism: evidence of underconnectivity. Brain. 127:1811–1821.

Kaufman L, Rousseeuw P. 1990. Finding Groups in Data: An Introduction to Cluster Analysis. Hoboken, NJ: John Wiley & Sons, Inc.

Khan S, Gramfort A, Shetty N, Kitzbichler M, Ganesan S, Moran J, Lee S, Gabrieli J, Tager-Flusberg H, Joseph R, et al. 2013. Local and long-range functional connectivity is reduced in concert in autism spectrum disorders. Proc Natl Acad Sci USA. 110:3107–3112.

Lee J, Kyeong S, Kim E, Cheon K. 2016. Abnormalities of inter- and intra-hemispheric functional connectivity in autism spectrum disorders: a study using the autism brain imaging data exchange database. Frontiers in Neuroscience. 10:191.

Lent R, Azevedo F, Andrade-Moraes C, Pinto A. 2012. How many neurons do you have? Some dogmas of quantitative neuroscience under revision. Eur J Neurosci. 35:1–9.

Liu X, Duyn J. 2013. Time-varying functional network information extracted from brief instances of spontaneous brain activity. Proc Natl Acad Sci USA. 110:4392–4397.

Lord C, Risi S, Lambrecht L, Cook EJ, Leventhal B, DiLavore P, Pickles A, Rutter M. 2000. The autism diagnostic observation schedule-generic: a standard measure of social and communication deficits associated with the spectrum of autism. J Autism Dev Disord. 30:205–223.

Lyall K, Croen L, Daniels J, Fallin M, Ladd-Acosta C, Lee B, Park B, Snyder N, Schendel D, Volk H, et al. 2016. The changing epidemiology of autism spectrum disorders. Annu Rev Public Health. doi:10.1146/annurev-publhealth-031816-044318.

Masi A, DeMayo M, Glozier N, Guastella A. 2017. An overview of autism spectrum disorder, heterogeneity and treatment options. Neurosci Bull. 33:183–193.

Mason M, Norton M, Van Horn J, Wegner D, Grafton S, Macrae C. 2007. Wandering minds: the default network and stimulus-independent thought. Science. 315:393–395.

Maximo J, Keown C, Nair A, Müller R. 2013. Approaches to local connectivity in autism using resting state functional connectivity MRI. Front Hum Neurosci. 7:605.

Minshew N, Goldstein G, Siegel D. 1997. Neuropsychologic functioning in autism: profile of a complex information processing disorder. Journal of the International Neuropsychological Society. 3:303–316.

Monk C, Peltier S, Wiggins J, Weng S, Carrasco M, Risi S, Lord C. 2009. Abnormalities of intrinsic functional connectivity in autism spectrum disorders. Neuroimage. 47:764–772.

Müller R. 2007. The study of autism as a distributed disorder. Ment Retard Dev Disabil Res Rev. 13:85–95.

Müller R, Shih P, Keehn B, Deyoe J, Leyden K, Shukla D. 2011. Underconnected, but How? A survey of functional connectivity MRI studies in autism spectrum disorders. Cereb Cortex. 21:2233–2243.

Nair A, Carper R, Abbott A, Chen C, Solders S, Nakutin S, Datko M, Fishman I, Müller R. 2015. Regional specificity of aberrant thalamocortical connectivity in autism. Hum Brain Mapp. 36:4497–4511.

Nair S, Jao Keehn R, Berkebile M, Maximo J, Witkowska N, Müller R. 2017. Local resting state functional connectivity in autism: site and cohort variability and the effect of eye status. Brain Imaging Behav. doi:10.1007/s11682-017-9678-y [Epub ahead of print].

Nair A, Treiber J, Shukla D, Shih P, Müller R. 2013. Impaired thalamocortical connectivity in autism spectrum disorder: a study of functional and anatomical connectivity. Brain. 136: 1942–1955.

Nielsen J, Zielinski B, Fletcher P, Alexander A, Lange N, Bigler E, Lainhart J, Anderson J. 2014. Abnormal lateralization of functional connectivity between language and default mode regions in autism. Mol Autism. 5:8.

Ozonoff S, Pennington B, Rogers S. 1991. Executive function deficits in high-functioning autistic individuals: relationship to theory of mind. J Child Psychol Psychiatry. 32:1081–1105.

Power J, Barnes K, Snyder A, Schlaggar B, Petersen S. 2012. Spurious but systematic correlations in functional connectivity MRI networks arise from subject motion. Neuroimage. 59:2142–2154.

Ray M, Graham A, Lee M, Perry R, Court J, Perry E. 2005. Neuronal nicotinic acetylcholine receptor subunits in autism: an immunohistochemical investigation in the thalamus. Neurobiol Dis. 19:366–377.

Risch N, Hoffmann T, Anderson M, Croen L, Grether J, Windham G. 2014. Familial recurrence of autism spectrum disorder: evaluating genetic and environmental contributions. Am J Psychiatry. 171:1206–1213.

Rubinov M, Sporns O. 2010. Complex network measures of brain connectivity: uses and interpretations. Neuroimage. 52:1059–1069.

Rutter M, LeCouteur A, Lord C. 2008. Autism diagnostic interview – Revised (ADI-R). Los Angeles: Western Psychological Services.

Schuetze M, Park M, Cho I, MacMaster F, Chakravarty M, Bray S. 2016. Morphological alterations in the thalamus, striatum, and pallidum in autism spectrum disorder. Neuropsychopharmacology. 41:2627–2637.

Sherman S, Guillery R. 2011. Distinct functions for direct and transthalamic corticocortical connections. J Neurophysiol. 106:1068–1077.

Shirer W, Ryali S, Rykhlevskaia E, Menon V, Greicius M. 2012. Decoding subject-driven cognitive states with whole-brain connectivity patterns. Cereb Cortex. 22:158–165.

Smith S, Jenkinson M, Woolrich M, Beckmann C, Behrens T, Johansen-Berg H, Bannister P, De Luca M, Drobnjak I, Flitney D, et al. 2004. Advances in functional and structural MR image analysis and implementation as FSL. Neuroimage. 23 (suppl 1):S208–S219.

Steinmetz H. 1996. Structure, function and cerebral asymmetry: in vivo morphometry of the planum temporale. Neurosci Biobehav Rev. 20:587–591.

Tomasi D, Shokri-Kojori E, Volkow N. 2016a. High-resolution functional connectivity density: hub locations, sensitivity, specificity, reproducibility, and reliability. Cereb Cortex. 26: 3249–3259.

Tomasi D, Shokri-Kojori E, Volkow N. 2016b. Temporal evolution of brain functional connectivity metrics: could 7 min of rest be enough? Cereb Cortex. doi:10.1093/cercor/bhw1227.

Tomasi D, Volkow N. 2010. Functional connectivity density mapping. Proc Natl Acad Sci USA. 107:9885–9890.

Tomasi D, Volkow N. 2011a. Aging and functional brain networks. Molecular Psychiatry. doi:10.1038/mp.2011.1081.

Tomasi D, Volkow N. 2011b. Association between functional connectivity hubs and brain networks. Cereb Cortex. 21: 2003–2013.

Tomasi D, Volkow N. 2011c. Functional connectivity hubs in the human brain. Neuroimage. 57:908–917.

Tomasi D, Volkow N. 2011d. Gender differences in brain functional connectivity density. Hum Brain Mapp. 33:849–860.

Tomasi D, Volkow N. 2012a. Abnormal functional connectivity in children with attention-deficit/hyperactivity disorder. Biol Psychiatry. 71:443–450.

Tomasi D, Volkow N. 2012b. Aging and functional brain networks. Mol Psychiatry. 17:549–558.

Tomasi D, Volkow N. 2012c. Laterality patterns of brain functional connectivity: gender effects. Cereb Cortex. 22:1455–1462.

Tomasi D, Volkow N. 2012d. Resting functional connectivity of language networks: characterization and reproducibility. Mol Psychiatry. 17:841–854.

Tomasi D, Volkow N. 2014a. Functional connectivity of substantia nigra and ventral tegmental area: maturation during adolescence and effects of ADHD. Cereb Cortex. 24:935–944.

Tomasi D, Volkow N. 2014b. Mapping small-world properties through development in the human brain: disruption in schizophrenia. Plos ONE. 9:e96176.

Tomasi D, Wang G, Volkow N. 2013. Energetic cost of brain functional connectivity. Proc Natl Acad Sci USA. 110:13642–13647.

Toro R, Konyukh M, Delorme R, Leblond C, Chaste P, Fauchereau F, Coleman M, Leboyer M, Gillberg C, Bourgeron T. 2010. Key role for gene dosage and synaptic homeostasis in autism spectrum disorders. Trends Genet. 26:363–372.

Travers B, Adluru N, Ennis C, Tromp do P, Destiche D, Doran S, Bigler E, Lange N, Lainhart J, Alexander A. 2012. Diffusion tensor imaging in autism spectrum disorder: a review. Autism Res. 5(289):313.

Tsatsanis K, Rourke B, Klin A, Volkmar F, Cicchetti D, Schultz R. 2003. Reduced thalamic volume in high-functioning individuals with autism. Biol Psychiatry. 53:121–129.

Tyszka J, Kennedy D, Paul L, Adolphs R. 2014. Largely typical patterns of resting-state functional connectivity in high-functioning adults with autism. Cereb Cortex. 24:1894–1905.

Van Dijk K, Sabuncu M, Buckner R. 2012. The influence of head motion on intrinsic functional connectivity MRI. Neuroimage. 59:431–438.

von dem Hagen E, Stoyanova R, Baron-Cohen S, Calder A. 2013. Reduced functional connectivity within and between 'social' resting state networks in autism spectrum conditions. Soc Cogn Affect Neurosci. 8:694–701.

Watanabe T, Rees G. 2017. Brain network dynamics in high-functioning individuals with autism. Nat Commun. 8:16048.

Weng S, Wiggins J, Peltier S, Carrasco M, Risi S, Lord C, Monk C. 2010. Alterations of resting state functional connectivity in the default network in adolescents with autism spectrum disorders. Brain Res. 1313:202–214.

Woodward N, Giraldo-Chica M, Rogers B, Cascio C. 2017. Thalamocortical dysconnectivity in autism spectrum disorder: an analysis of the Autism Brain Imaging Data Exchange. Biol Psychiatry Cogn Neurosci Neuroimaging. 2:76–84.

Yang H, Long X, Yang Y, Yan H, Zhu C, Zhou X, Zang Y, Gong Q. 2007. Amplitude of low frequency fluctuation within visual areas revealed by resting-state functional MRI. Neuroimage. 36:144–152.

Zikopoulos B, Barbas H. 2010. Changes in prefrontal axons may disrupt the network in autism. J Neurosci. 30: 14595–14609.